

Polythiophenes comprising conjugated pendants toward long-term air-stable inverted polymer solar cells with high open circuit voltages

Cite this: *J. Mater. Chem. A*, 2013, **1**, 8950

Hsing-Ju Wang,^a Chen-Wei Chou,^b Chih-Ping Chen,^{*c} Ying-Hsiao Chen,^b Rong-Ho Lee^{*b} and Ru-Jong Jeng^{*a}

A series of polythiophenes (PTs) functionalized with bulky conjugated side chains comprising *tert*-butyl substituted carbazole (tCz) as an electron donor pendant and bisbenzothiazolylvinyl (DBT) as an electron acceptor pendant were synthesized via Stille copolymerization for polymer solar cell (PSC) applications. We use the descriptors PTtCz, PT(tCz)_{0.9}(DBT)_{0.1}, PT(tCz)_{0.64}(DBT)_{0.36}, PT(tCz)_{0.45}(DBT)_{0.55}, and PTDBT to identify each of these conjugated polymers, with the names denoting the compositions of the bulky pendants. The tunable energy levels of the PTs were accomplished by incorporating both tCz as a donor pendant and DBT as an acceptor pendant, while retaining the low-lying HOMO levels (−5.26 to −5.39 eV). Furthermore, lower bandgaps were observed for the DBT-derived PTs because of stronger donor– π –acceptor characteristics and more efficient intramolecular charge transfer. Conventional PSCs were fabricated by spin-coating the blend of each PT and the fullerene derivative (PC₇₁BM). The conventional PSC devices exhibited high open circuit voltages (V_{oc}) of around 0.79–0.91 V. The power conversion efficiency (PCE) of the PSCs based on PTtCz : PC₇₁BM (w/w = 1 : 2.5) reached 2.48% with a V_{oc} of 0.91 V, short circuit current (J_{sc}) of 6.58 (mA cm^{−2}) and fill factor (FF) of 41% under the illumination of AM1.5, 100 mW cm^{−2}. Furthermore, a PTtCz/PC₇₁BM-based inverted PSC with ZnO_x and MoO₃ as an electron extraction layer and a hole extraction layer respectively was capable of retaining ca. 80% of its original efficiency after storage under ambient conditions (without encapsulation) for 1032 h, according to the ISOS-D-1 shelf protocol. The highly durable inverted PSC accompanied by a large V_{oc} value was achieved for the PT-type polymers.

Received 29th March 2013
Accepted 16th May 2013

DOI: 10.1039/c3ta11272a

www.rsc.org/MaterialsA

Introduction

Wet-processing is the main advantage of polymer solar cells (PSC). In this process, the active layer can be manufactured using fast roll-to-roll based methods at a cost that has the potential to be competitive, pending further development.^{1–5} On the basis of the concept of the bulk heterojunction (BHJ) structure, PSCs made by blending poly(3-hexylthiophene) (P3HT) as a donor and fullerene derivative [6,6]-phenyl-C₆₁/71-butyric acid methyl ester (PC₆₁BM/PC₇₁BM) as an acceptor have been intensively investigated, leading to power conversion efficiencies (PCE) of up to 4–5%.^{6–8} Unfortunately, the highest occupied molecular orbital (HOMO) (−4.9 to −5.1 eV) energy level of P3HT resulted in an unsatisfactory open circuit voltage

(V_{oc}) value of only about 0.6 V and narrow absorption spectra in the UV-visible region which limited the photocurrent generation of its related BHJ solar cell.⁹ In general, the V_{oc} of a PSC is proportional to the difference between the HOMO of the electron-sufficient polymer and the lowest unoccupied molecular orbital (LUMO) of the electron-deficient fullerene. Lower HOMO levels of the polymers would provide a higher V_{oc} according to the theoretical prediction. Additionally, conjugated polymers with higher ionization potentials are capable of minimizing the p-doping level under ambient O₂ and increasing the environmental stability.¹⁰

Much of the improvement in PSCs can be attributed to the design of novel conjugated polymers with (i) strong and broad visible absorption with high charge carrier mobility to increase the short-circuit current density (J_{sc}) and (ii) low-lying HOMO levels to achieve large V_{oc} values. The absorption properties and the energy levels can be modulated by introducing conjugated side chains onto the conjugated polymers.^{11,12} Li and coworkers first studied a PT with conjugated pendants attached that exhibited a broad absorption band in the UV and visible regions, and was capable of harvesting a great amount of solar light.¹³ Subsequently, the investigations on PTs comprising

^aInstitute of Polymer Science and Engineering, National Taiwan University, Taipei 106, Taiwan. E-mail: rujong@ntu.edu.tw; Fax: +886-2-33665237; Tel: +886-2-33665884

^bDepartment of Chemical Engineering, National Chung Hsing University, Taichung 402, Taiwan. E-mail: rhl@nchu.edu.tw; Fax: +886-4-22854734; Tel: +886-4-22854308

^cDepartment of Materials Engineering, Ming Chi University of Technology, New Taipei City 243, Taiwan. E-mail: cpchen@mail.mcut.edu.tw; Fax: +886-2-29084091; Tel: +886-2-29089899 extn. 4439

conjugated pendants as side-chains have attracted a great deal of interest.^{14–19} Our previous studies on conjugated polymers presenting bulky conjugated electron donor moieties as side-chains revealed that the sterically induced twisting of the polymer backbone was responsible for achieving a low-lying HOMO level and enhancing the oxidative stability of conjugated polymers as compared to the parent P3HT.^{20,21} Larger V_{oc} values of the conjugated PTs functionalized with bulky pendants have been observed in conventional PSCs.^{13,22–24} Nevertheless, the bulky substituents increase the degree of twisting from planarity in the backbone, resulting in a decreased intramolecular charge transfer and larger optical bandgaps (E_g). To address this issue, the incorporation of electron acceptor pendants on PTs was studied by Wei and coworkers.^{17,18} The results showed that a lower E_g was obtained due to the presence of the efficient intramolecular charge transfer from the PT backbone to the conjugated acceptor side chain induced by the electron-accepting imidazole moiety.

To systematically investigate the variation of photophysical properties and energy levels *via* the strategy of developing PTs with covalently attached both electron donor and acceptor pendants, we first synthesized PTs functionalized with various contents of *tert*-butyl substituted carbazole (*tCz*) as an electron donor pendant^{25,26} and bisbenzothiazolylvinyl (DBT) as an electron acceptor pendant.^{27,28} The synthesis, properties and PSC performances of the novel PTs comprising 2-ethylhexyl-substituted quaterthiophene (T) as the conjugated unit in the PT backbone along with different composition ratios of *tCz* and DBT as bipolar pendant groups were reported in this study (Scheme 1). According to the literature,²⁹ the optical and electronic properties of the polymers can be easily manipulated through the attachment of electron-withdrawing groups while taking the variation of the acceptor strengths into account. Therefore, one would anticipate further energy level adjustment when the acceptor moiety DBT is incorporated. Depending on the copolymer composition of PTs comprising conjugated pendants, samples such as PT*tCz*, PT(*tCz*)_{0.9}(DBT)_{0.1}, PT(*tCz*)_{0.64}(DBT)_{0.36}, PT(*tCz*)_{0.45}(DBT)_{0.55}, and PTDBT were synthesized and investigated (Scheme 1). To validate the dual-adjustment of the lower-lying HOMO levels and narrow E_g values, UV-vis absorption spectroscopy and cyclic voltammetry (CV) were employed to study the effect of bipolar pendants on the photophysical and electrochemical properties of the PT-based copolymers. We fabricated conventional PSCs by spin-coating the solutions of PT-based

copolymers/PC₇₁BM blends, and then the dried films were sandwiched between a transparent anode ITO and cathodes (Ca/Al). The PV performance of these PSCs was studied in terms of the influence of the conjugated pendant groups. Additionally, in order to investigate the important issue of air stability, the PT*tCz* based inverted devices without encapsulation were tested under ambient conditions for 1032 h, under the ISOS-D-1 shelf measurement.^{30,31}

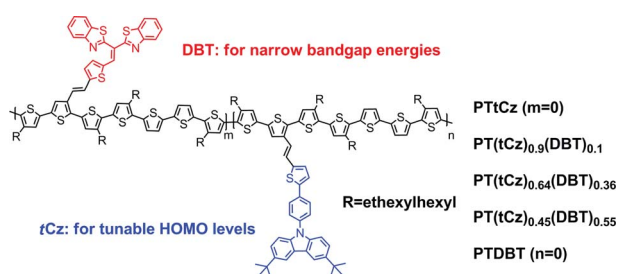
Experimental

Chemicals

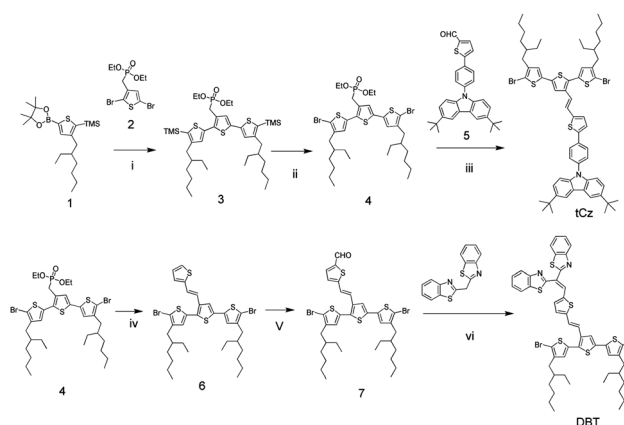
Trimethylstannyl chloride, *n*-bromosuccinimide, 2-formylthiophene, phosphorous oxychloride, 2,2'-methylene bisbenzothiazole, *n*-butyllithium (2.5 M in hexane) and other reagents and chemicals were purchased from Aldrich, Alfa and TCI Chemical Co., and used as received. Dichloromethane (DCM), tetrahydrofuran (THF), dimethylformamide (DMF), toluene, and *o*-dichlorobenzene (*o*-DCB) were freshly distilled over appropriate drying agents prior to use, while being purged with nitrogen. The *tert*-butyl-substituted carbazole-containing moiety (*tCz*) and 2, 2'-methylenebisbenzothiazole substituted moiety (DBT) were synthesized according to Scheme 2. Syntheses of a series of PTs-based donor-acceptor random copolymers *via* Stille polymerization with various *tCz*/DBT feed ratios are illustrated in Scheme 3. Compounds 2-(4-ethylhexyl-5-trimethylsilylthiophen-2-yl)-4,4,5,5-tetramethyl-1,3,2]dioxaborolane (1), diethyl(2,5-dibromothiophen-3-yl)methylphosphonate (2), 5-(4-(3,6-di-*tert*-9-carbazolyl)phenyl)thiophene-2-carbaldehyde (5) and 5,5'''-dibromo-3,3'''-diethylhexyl-2,2'; 5',2''; 5'',2'''-quater-thiophene were synthesized according to the literature.^{22,32}

Synthesis of compound (3)

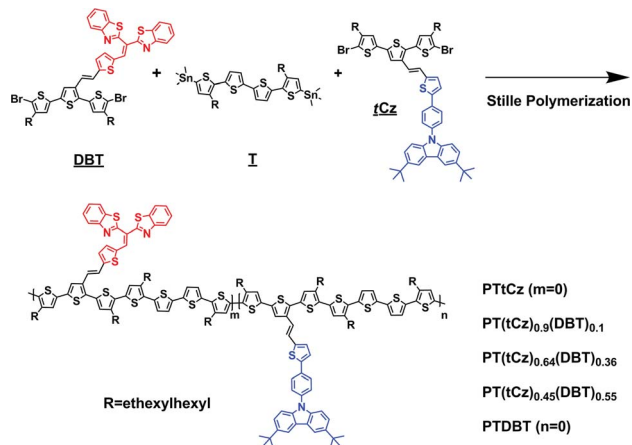
A mixture of compound (2) (0.58 g, 1.5 mmol), compound (1) (1.21 g, 3.3 mmol), and Pd(PPh₃)₄ (0.037 g, 0.03 mmol) was dissolved in a degassed mixture of toluene (12 mL) and 2 M



Scheme 1 PTs comprising bipolar pendant groups.



Scheme 2 Synthesis of the conjugated pendants *tCz* and DBT (i) Pd(PPh₃)₄, 2M K₂CO₃ (aq.), toluene, reflux, 8 h; (ii) NBS, AcOH, DCM, 0 °C, 1 h; (iii) CH₃ONa, DMF, 0 °C, 2 h; (iv) 2-carboxaldehyde, potassium *tert*-butoxide, THF, 0 °C, 1 h; (v) DMF, phosphoryl chloride, dichloroethane, from 0 °C to reflux, 8 h; (vi) 2,2'-methylenebisbenzothiazole, I₂, K₂CO₃, DMF, 60 °C, 6 h.



Scheme 3 Reaction scheme for preparing the PT-based random copolymers.

$\text{K}_2\text{CO}_3(\text{aq})$ (12 mL). The solution was stirred at reflux temperature for 48 h, and then poured into methanol (100 mL). The crude product was partitioned between EA and water, and the organic phase was dried (MgSO_4), filtered, and evaporated to dryness. The residue was purified using silica gel chromatography (EA : hexane = 1 : 10) to give a yellow liquid (0.72 g, yield = 63%). $^1\text{H-NMR}$ (δ/ppm , CDCl_3): 0.28 (s, 18H), 0.84 (m, 18H), 1.22 (m, 16H), 1.55 (m, 2H), 2.58 (m, 4H), 3.25 (d, $J = 6.4$ Hz, 2H), 4.02 (m, 4H), 7.05 (s, 1H), 7.15 (m, 2H).

Synthesis of compound (4)

Compound (3) (6.22 g, 10 mmol) was dissolved in DCM (25 mL). The solution was then stirred in an ice water bath for 15 minutes. *N*-bromosuccinimide (3.55 g, 20 mmol) was dissolved in a mixture of DCM (20 mL) and AcOH (10 mL). This mixture was then added dropwise to the compound (3) solution over 15 min at 0 °C. The reaction mixture was warmed to room temperature and stirred for 2 h. Subsequently, Na_2SO_3 aqueous solution was added to quench the reaction. The mixture was partitioned between EA–water, and the organic phase was dried (MgSO_4), filtered, and evaporated to dryness. The residue was purified using silica gel chromatography (EA : hexane = 1 : 10) to give a yellow liquid (5.72 g, yield = 81%). $^1\text{H-NMR}$ (δ/ppm , 400 MHz, CDCl_3): 0.86 (m, 18H), 1.23 (m, 16H), 1.58 (m, 2H), 2.42 (m, 4H), 3.18 (d, $J = 5.2$ Hz, 2H), 4.02 (m, 4H), 6.80 (s, 1H), 6.84 (s, 1H), 7.08 (s, 1H).

Synthesis of compound tCz

A mixture of compound (4) (7.81 g, 10 mmol) and CH_3ONa (1.78 g, 33 mmol) in 30 mL DMF was stirred under an ice water bath for several minutes. Compound (5) (4.66 g, 10 mmol) was then added to the solution. After 2 h, the reaction was quenched with methanol and a yellow powder was precipitated. Further purification was performed using silica gel chromatography (hexane as eluent) to give a yellow solid (7.19 g, yield = 66%). $^1\text{H-NMR}$ (δ/ppm , 400 MHz, CDCl_3): 0.82 (m, 12H), 1.29 (m, 16H), 1.44 (s, 18H), 1.59 (m, 2H), 2.48 (m, 4H), 6.85 (d, $J = 1.2$ Hz, 2H), 7.07 (m, 3H), 7.25 (d, $J = 8.8$ Hz, 1H), 7.28 (d, $J = 7.6$ Hz, 1H),

7.38 (d, $J = 0.8$ Hz, 2H), 7.44 (m, 2H), 7.54 (d, $J = 9.2$ Hz, 2H), 7.77 (d, $J = 4$ Hz, 2H), 8.12 (t, $J = 1.6$ Hz, 2H). ESIMS (m/z): calcd for $\text{C}_{60}\text{H}_{69}\text{Br}_2\text{NS}_4$: 1092.26. Found: 1092.4. Anal calcd for $\text{C}_{50}\text{H}_{50}\text{Br}_2\text{N}_2\text{S}_6$: C, 65.98; H, 6.37; N, 1.28. Found: C, 65.72; H, 6.44; N, 1.14%.

Synthesis of compound (6)

A mixture of compound (4) (7.81 g, 10 mmol) and K_2CO_3 (2.76 g, 20 mmol) in 30 mL dry THF was stirred under an ice water bath for 15 minutes. A solution of 2-carbadehydethiophene (1.68 g, 15 mmol) in dry THF (7 mL) was then added to the mixture. After 2 h, the reaction was quenched with methanol. Further purification was performed using silica gel chromatography (hexane as eluent) to give a yellow oil (4.95 g, yield = 67%). $^1\text{H-NMR}$ (δ/ppm , 400 MHz, CDCl_3): 0.87 (m, 12H), 1.27 (m, 16H), 1.52 (m, 2H), 2.45 (m, 4H), 6.81 (d, $J = 10$ Hz, 1H), 6.98 (m, $J = 8.4$ Hz, 1H), 7.02 (s, 1H), 7.05 (s, 1H), 7.08 (d, $J = 3.2$ Hz, 1H), 7.14 (s, 1H), 7.19 (d, $J = 5.2$ Hz, 1H), 7.23 (d, $J = 3.6$ Hz, 1H).

Synthesis of compound (7)

POCl_3 (7.45 mL, 80 mmol) was added dropwise to freshly distilled DMF (3.09 mL, 40 mmol) at 0 °C under nitrogen atmosphere. Compound 6 (7.39 g, 10 mmol) dissolved in dichloroethane (50 mL) was added dropwise to the above-mentioned POCl_3/DMF complex at room temperature. The reaction mixture was stirred at 80 °C for 3 h. Subsequently, the reaction was cooled to 0 °C and 2 M NaOH aqueous solution was added to quench the reaction. The mixture was partitioned between EA–water, and the organic phase was dried (MgSO_4), filtered, and evaporated to dryness. The residue was purified using silica gel chromatography (EA : hexane = 1 : 10) to give a yellow oil (5.09 g, 77%). $^1\text{H-NMR}$ (δ/ppm , 400 MHz, CDCl_3): 0.86 (m, 12H), 1.27 (m, 16H), 1.59 (m, 2H), 2.45 (m, 4H), 6.81 (d, $J = 10.4$ Hz, 1H), 7.06 (s, 1H), 7.10 (s, 1H), 7.12 (d, $J = 2.8$ Hz, 1H), 7.23 (d, $J = 2.4$ Hz, 1H), 7.25 (d, $J = 4.0$ Hz, 1H), 7.63 (d, $J = 5.6$ Hz, 1H), 9.89 (s, 1H).

Synthesis of compound DBT

A mixture of dibenzo[d]thiazol-2-ylmethane (3.11 g, 11 mmol), K_2CO_3 (0.04 g, 0.3 mmol), and I_2 (0.07 g, 0.3 mmol) in 20 mL DMF was stirred under room temperature for 15 minutes. A solution of compound 7 (7.67 g, 10 mmol) in DMF (15 mL) was added to the mixture, and then the reaction solution was heated to 60 °C. After 2 h, the reaction was quenched with methanol. The mixture was partitioned between EA–water, and the organic phase was dried (MgSO_4), filtered, and evaporated to dryness. Further purification was performed using silica gel chromatography (EA : hexane = 1 : 10) to give a red solid (7.43 g, yield = 72%). $^1\text{H-NMR}$ (δ/ppm , CDCl_3): 0.86 (m, 12H), 1.28 (m, 16H), 1.54 (m, 2H), 2.43 (m, 4H), 6.76 (d, $J = 8.0$ Hz, 2H), 6.87 (s, 1H), 6.91 (d, $J = 13.6$ Hz, 1H), 6.98 (d, $J = 6.4$ Hz, 2H), 7.15 (s, 1H), 7.19 (t, $J = 4.4$ Hz, 1H), 7.31 (t, $J = 16.4$ Hz, 1H), 7.49 (t, $J = 12.8$ Hz, 2H), 7.55 (t, $J = 16.8$ Hz, 1H), 7.79 (d, $J = 7.6$ Hz, 1H), 7.99 (d, $J = 8$ Hz, 2H), 8.16 (s, 1H), 8.22 (d, $J = 8.4$ Hz, 1H). ESIMS (m/z): calcd for $\text{C}_{50}\text{H}_{50}\text{Br}_2\text{N}_2\text{S}_6$: 1031.14 Found: 1031.0. Anal

calcd for $C_{50}H_{50}Br_2N_2S_6$: C, 58.24; H, 4.89; N, 2.72; S, 18.66
Found: C, 58.24; H, 4.86; N, 2.77; S, 18.52%.

Synthesis of compound T

A solution of 5,5'''-dibromo-3,3'''-diethylhexyl-2,2'; 5',2''; 5'',2'''-quaterthiophene (7.12 g, 10 mmol) in dry THF (150 mL) was stirred at -78°C under a N_2 atmosphere and then *n*-BuLi (2.5 M in hexane, 8.40 mL, 21 mmol) was added dropwise to the solution. The solution mixture was maintained at -78°C with stirring for 1 h, at which point trimethyltinchloride (4.98 g, 25 mmol) in dry THF (5 mL) was added dropwise. The mixture was warmed to room temperature and stirred for 8 h. Subsequently, HCl (1 N) was added to quench the reaction. The resulting mixture was partitioned between EA and water, and the organic phase was dried ($MgSO_4$), filtered, and evaporated to dryness. The residue was purified using silica gel chromatography (hexane, with 1% TEA) to give a greenish oil (7.13 g, yield = 81%). $^1\text{H-NMR}$ (δ /ppm, 400 MHz, $CDCl_3$): 0.82 (m, 12H), 1.07 (m, 18H), 1.23 (m, 16H), 1.52 (m, 2H), 2.71 (m, 4H), 6.89 (s, 2H), 6.98 (d, $J = 3.6$ Hz, 2H), 7.08 (d, $J = 4$ Hz, 2H). ESIMS (m/z): calcd for $C_{38}H_{58}S_4Sn_2$: 880.55 Found: 880.2. Anal calcd for $C_{38}H_{58}S_4Sn_2$: C, 51.83; H, 6.64 Found: C, 52.10; H, 6.74%.

Synthesis of PTtCz

A solution of tCz (1.64 g, 1.5 mmol) and T (1.32 g, 1.5 mmol) in dry toluene (20 mL) was purged with N_2 and subjected to three freeze–pump–thaw cycles to remove traces of O_2 . $Pd(PPh_3)_4$ (30 mg, 1 mol%) was added to the mixture, which was then stirred and heated under reflux for 48 h. After cooling to room temperature, the mixture was poured into MeOH (100 mL) and the precipitated material was filtered through a Soxhlet thimble. Soxhlet extractions were performed sequentially with MeOH, hexane, acetone, and $CHCl_3$. The polymer was recovered through rotary evaporation of the $CHCl_3$ fraction. Drying the sample under vacuum for 24 h provided an orange–red solid (70%). Gel permeation chromatography (GPC; THF): weight-average molecular weight (M_w), 21 421 $g\ mol^{-1}$; polydispersity index (PDI), 2.35. $^1\text{H-NMR}$ (δ /ppm, 400 MHz, $CDCl_3$): 1.01 (br, 42H), 1.30–1.34 (br, 32H), 1.57–1.62 (br, 4H), 2.30–2.46 (br, 8H), 6.40–7.50 (br, 15H), 7.55 (br, 2H), 7.79 (br, 2H), 8.12 (br, 4H).

Synthesis of PT(tCz)_{0.9}(DBT)_{0.1}

Using the same procedure as that described for the synthesis of PTtCz, the reaction of tCz (1.24 g, 1.13 mmol), DBT (0.38 g, 0.37 mmol), and T (1.32 g, 1.5 mmol) gave a dark-red solid (67%). GPC: M_w , 41 531 $g\ mol^{-1}$; PDI, 3.49. $^1\text{H-NMR}$ (δ /ppm, 400 MHz, $CDCl_3$): 1.01 (br, 84H), 1.30–1.34 (br, 64H), 1.57–1.62 (br, 8H), 2.60–2.80 (br, 16H), 6.40–7.50 (br, 33H), 7.55 (br, 2H), 7.79 (br, 3H), 7.88 (br, 1H), 7.99 (br, 1H), 8.16 (br, 4H), 8.22 (br, 1H).

Synthesis of PT(tCz)_{0.64}(DBT)_{0.36}

Using the same procedure as that described for the synthesis of PTtCz, the reaction of tCz (0.82 g, 0.75 mmol), DBT (0.77 g, 0.75 mmol), and T (1.32 g, 1.5 mmol) gave a dark-red solid (64%). GPC: M_w , 34 235 $g\ mol^{-1}$; PDI, 3.23. $^1\text{H-NMR}$ (δ /ppm, 400 MHz,

$CDCl_3$): 0.87 (br, 84H), 1.26–1.30 (br, 64H), 1.45–1.56 (br, 8H), 2.62–2.84 (br, 16H), 6.94–7.46 (br, 33H), 7.56 (br, 2H), 7.80 (br, 3H), 7.89 (br, 1H), 8.01 (br, 1H), 8.14 (br, 4H), 8.19 (br, 1H).

Synthesis of PT(tCz)_{0.45}(DBT)_{0.55}

Using the same procedure as that described for the synthesis of PTtCz, the reaction of tCz (0.40 g, 0.37 mmol), DBT (1.16 g, 1.13 mmol), and T (1.32 g, 1.5 mmol) gave a dark-red solid (60%). GPC: M_w , 28 875 $g\ mol^{-1}$; PDI, 2.93. $^1\text{H-NMR}$ (δ /ppm, 400 MHz, $CDCl_3$): 0.88 (br, 84H), 1.27–1.30 (br, 64H), 1.46–1.70 (br, 8H), 2.72 (br, 16H), 6.95–7.46 (br, 33H), 7.57 (br, 2H), 7.80 (br, 3H), 7.91 (br, 1H), 8.01 (br, 1H), 8.14 (br, 4H), 8.20 (br, 1H).

Synthesis of PTDBT

Using the same procedure as that described for the synthesis of PTtCz, the reaction of DBT (1.54 g, 1.5 mmol) and T (1.32 g, 1.5 mmol) gave a dark-red solid (65%). GPC: M_w , 29 616 $g\ mol^{-1}$; PDI, 3.49. $^1\text{H-NMR}$ (δ /ppm, 400 MHz, $CDCl_3$): 0.89 (br, 84H), 1.30–1.34 (br, 64H), 1.57–1.62 (br, 8H), 2.47–2.80 (br, 16H), 6.90–7.31 (br, 18H), 7.77 (br, 1H), 7.88 (br, 1H), 7.98 (br, 1H), 8.17 (br, 1H).

Characterization of copolymers

$^1\text{H-NMR}$ (400 MHz) spectra were recorded using a Varian Unity Inova spectrometer. The average molecular weights of the polymers were measured by means of GPC on a Waters chromatography system (717 plus Autosampler) equipped with two Waters Styragel linear columns. Polystyrene standards were used, with THF as the eluent. The glass transition temperature (T_g) and thermal decomposition temperature (T_d , the temperature at which weight loss reaches 5%) of the copolymers were determined by means of differential scanning calorimetry (TA Instruments, DSC-2010) and thermogravimetric analysis (TA Instruments, TGA-2050), respectively. Both analyses were performed under N_2 atmosphere at a scanning (both heating and cooling) rate of $10^\circ\text{C}\ \text{min}^{-1}$. The absorption spectra were measured using a Hitachi U3010 UV-Vis spectrometer. Fluorescence spectra were measured using a Varian Cary Eclipse luminescence spectrometer. Dilute *o*-DCB solutions of the PTs were filtered through a 0.45 μm filter to remove insoluble materials before spectral measurements. Redox potentials of the polymers were determined with a CHI 611D electrochemical analyser (scanning rate: $50\ \text{mV}\ \text{s}^{-1}$) equipped with Pt electrodes and an Ag/Ag^+ (0.10 M $AgNO_3$ in MeCN) reference electrode in an anhydrous, N_2 -saturated solution of 0.1 M Bu_4NClO_4 in MeCN. Bu_4NClO_4 (98%, TCI) was recrystallized three times from ethyl acetate and then dried at 60°C under reduced pressure. A Pt plate coated with a thin polymer film was used as the working electrode, a Pt wire and an Ag/Ag^+ electrode were used as the counter and reference electrodes, respectively. CV curves were calibrated using ferrocene as the standard, whose HOMO is set at $-4.8\ \text{eV}$ with respect to zero vacuum level. The $E_{\text{onset}}^{\text{ox}}$ of ferrocene/ferrocene $^+$ is 0.36 V in $Bu_4NClO_4/MeCN$ solution (0.1 M). The HOMO energy levels were obtained from the equation: $\text{HOMO} = -e(E_{\text{onset}}^{\text{ox}} - E_{\text{onset,ferrocene}}^{\text{ox}} + 4.8)$ (eV). The

LUMO levels of the polymer were obtained from the equation:

$$\text{LUMO} = -e(E_{\text{onset}}^{\text{red}} - E_{\text{onset,ferrocene}}^{\text{red}} + 4.8) \text{ (eV)}.$$
³³

Fabrication and characterization of PSCs³⁴

All the conventional PSCs in this study were based on a structure like the indium tin oxide (ITO)-coated glass/hole-transporting material (HTM)/photoactive layer/Ca (30 nm)/Al (100 nm) structure, in which the photoactive layer consisted of an interpenetrating network of PTs/PC₇₁BM. The ITO substrates (obtained from Sanyo, Japan ($8 \Omega \square^{-1}$)) were first patterned by lithography, cleaned with detergent, and ultrasonicated in acetone and isopropyl alcohol, dried on a hot plate at 120 °C for 5 min, and finally treated with oxygen plasma for 5 min. PC₇₁BM was purchased from Nano-C and used as received. Poly(3,4-ethylene-dioxythiophene):poly(styrenesulfonate) (PEDOT:PSS, Baytron P-VP A14083) was filtered through a 0.45 μm filter before being deposited on ITO, with a thickness around 30 nm, by spin coating at 3000 rpm in the air and drying at 150 °C for 30 min inside a glove box. A solution mixture of PTs-based donor-acceptor random copolymers and PC₇₁BM (10 mg mL⁻¹ in *o*-DCB) was stirred overnight, then filtered through a 0.2 μm poly(tetrafluoroethylene) (PTFE) filter and spin-coated (1200 rpm, 30 s) onto the PEDOT:PSS layer to prepare the PT/PC₇₁BM composite film-based photo-active layer. The optimal thickness of the active layers obtained under these conditions was *ca.* 60 nm. Subsequently, the device was completed by depositing *ca.* (30 nm) and Al (100 nm) under $<10^{-6}$ mm-Hg pressure, respectively. The active area of the conventional device was 5 mm². Finally the cell was encapsulated using UV-curing glue (obtained from Nagase, Japan). During the encapsulation process, the UV-glue was dispensed onto the edge of a piece of glass in the air. The UV-glue coated glass was transferred to the glove box for covering the PSC device. The device was then sealed by pressing the UV-glue coated glass on top of the device, and the device underwent UV curing (254 nm) for 2 min. Upon device encapsulation, the *I-V* curves of the PSC devices were measured in an ambient atmosphere at 25 °C using a computer-controlled Keithley 2400 source measurement unit (SMU) equipped with a Peccell solar simulator under AM 1.5G illumination (100 mW cm⁻²). The illumination intensity was calibrated using a standard Si photodiode detector equipped with a KG-5 filter. The output photocurrent was adjusted to match the photocurrent of the Si reference cell to obtain a power density of 100 mW cm⁻². An inverted device of PT*t*Cz/PC₇₁BM-based film with the structure of ITO/ZnO_x/PT*t*Cz:PC₇₁BM/MoO₃/Ag, in which ITO acted as the cathode and Ag as the anode, was prepared using the following procedure. A ZnO_x precursor solution was spin-cast on top of the pre-cleaned ITO-glass substrate. The films were annealed at 150 °C for 1 h in air. The ZnO_x film thickness was approximately 30 nm, as determined by a profilometer. The ZnO_x-coated substrates were then placed in a glove box. A photoactive layer, PT*t*Cz:PC₇₁BM, was fabricated according to the condition for preparing the conventional device. Subsequently, a thin MoO₃ layer with a thickness of approximately 7 nm was vacuum-deposited on the top of the photoactive layer with an evaporation rate of 0.1 Å s⁻¹. In addition, the top electrode Ag

(50 nm) was thermally-deposited through a shade mask with an effective device area of 3 mm². The use of metal oxides on both sides of the PT*t*Cz:PC₇₁BM layer would prevent the diffusion of moisture into the active layer. Under ambient atmosphere, the measurements of long-term photovoltaic characteristics of the PT*t*Cz-derived inverted devices without encapsulation were performed in the same manner as those of the conventional devices as described above.

Results and discussion

Characterization of conjugated polymers

The molar ratios (*m/n*; Fig. 1) of the PTs were manipulated by controlling the feed ratios of the *t*Cz/DBT conjugation units. In addition, the actual values of *m/n* were determined from the relative integral areas attributed to the peaks of *t*Cz (7.48–7.50 ppm) and DBT (7.77–7.98 ppm and 8.17 ppm) by ¹H NMR spectra.^{22,28} The characteristic signals of *t*Cz and DBT moieties are shown in Fig. 1 and indicated as blue and red arrows, respectively. The copolymer compositions were determined and named according to the actual ratios as indicated by PT*t*Cz,

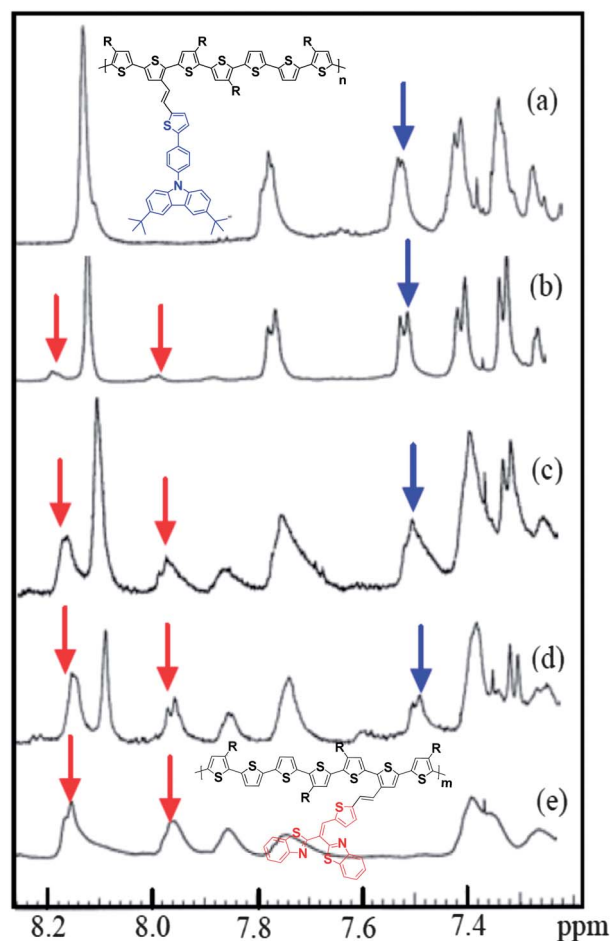


Fig. 1 ¹H NMR spectra of the PTs-based donor-acceptor random copolymers (a) PT*t*Cz, (b) PT(*t*Cz)_{0.9}(DBT)_{0.1}, (c) PT(*t*Cz)_{0.64}(DBT)_{0.36}, (d) PT(*t*Cz)_{0.45}(DBT)_{0.55}, and (e) PTDBT. The blue and red arrows indicate the characteristic signals of the *t*Cz and DBT moieties, respectively.

PT(*t*Cz)_{0.9}(DBT)_{0.1}, PT(*t*Cz)_{0.64}(DBT)_{0.36}, PT(*t*Cz)_{0.45}(DBT)_{0.55}, and PTDBT. It is important to note that a higher actual *m/n* ratio was obtained despite the equal *t*Cz/DBT feed ratio during polymerization, for example in the case of PT(*t*Cz)_{0.64}(DBT)_{0.36}. This might be due to the fact that the relatively poor solubility of the DBT bulky segment would inhibit the propagation of the polymer chains. Furthermore, a higher content of DBT-containing segments would also lead to precipitation at the initial stages of polymerization, resulting in better propagation of the *t*Cz-containing segment. All of the conjugated copolymers were soluble in common organic solvents, including chloroform, THF, and *o*-DCB. In general, conjugated polymers exhibit poor solubility due to strong π - π interaction between planar polymer backbones. Moreover, the presence of the branched 2-ethylhexyl side-chains is effective in improving the solubility of conjugated copolymers. Using GPC with THF as the eluent and calibrating by a polystyrene standard, we determined the weight-average molecular weights (M_w s) and PDIs of the conjugated PTs. The values of M_w and PDI of PT*t*Cz, PT(*t*Cz)_{0.9}(DBT)_{0.1}, PT(*t*Cz)_{0.64}(DBT)_{0.36}, PT(*t*Cz)_{0.45}(DBT)_{0.55}, and PTDBT were (21 421, 2.35), (41 531, 3.49), (34 235, 3.23), (28 875, 2.93), and (29 616, 2.29), respectively.

The operational stability of the PSCs is directly related to the thermal stability of the conjugated polymers. Thus, high T_g s and T_d s are desirable for the conjugated polymers. T_d s (taken at 5 wt% weight loss) of PT*t*Cz, PT(*t*Cz)_{0.9}(DBT)_{0.1}, PT(*t*Cz)_{0.64}(DBT)_{0.36}, PT(*t*Cz)_{0.45}(DBT)_{0.55}, and PTDBT were 367, 348, 331, 355, and 288 °C, respectively. T_g s were determined from the second round of DSC heating scans. The T_g s of PT*t*Cz, PT(*t*Cz)_{0.9}(DBT)_{0.1}, PT(*t*Cz)_{0.64}(DBT)_{0.36}, PT(*t*Cz)_{0.45}(DBT)_{0.55}, and PTDBT were 122, 132, 120, 133, and 122 °C, respectively, which are considered to be good candidates for PSC applications in terms of thermal stability. A single endothermic glass transition was observed for each conjugated copolymer, implying that the electron-donating and electron-withdrawing bulky pendants (*t*Cz and DBT) were distributed homogeneously.

Optical properties of the conjugated polymers

The normalized UV-vis absorption spectra of the PTs in *o*-DCB solution and as solid films are shown in Fig. 2. Table 1 summarizes the photophysical properties of the copolymers. As shown in Fig. 2(a), the absorption bands of the PTs in *o*-DCB ranged from 325 to 600 nm, and each polymer exhibited a single broad absorption band. In general, PTs functionalized with conjugated pendants exhibit two maximum absorption peaks, one in the visible region attributed to the π - π^* transition of the conjugated polymer main chains, and the other in the UV region attributed to the conjugated side chains.^{16,35} In this study, the PTs functionalized with conjugated *t*Cz/DBT moieties showed only a single broad absorption peak. This indicates that a high degree of intramolecular conjugation was present within the conjugated frameworks of the polymers when in solution. Due to the electron withdrawing characteristic of the DBT moiety, the maximum absorption band located in the longer wavelength region would generally take place.^{27,28} Further red-shift of the maximum absorption wavelengths (Table 1) for the copolymer

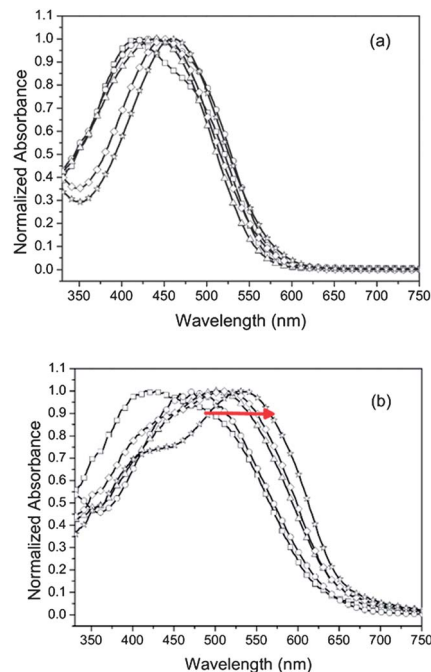


Fig. 2 UV spectra of PT-based random copolymers (a) in *o*-DCB and (b) as thin films. The symbols of the PTs are indicated as the following: PT*t*Cz (□), PT(*t*Cz)_{0.9}(DBT)_{0.1} (○), PT(*t*Cz)_{0.64}(DBT)_{0.36} (Δ), PT(*t*Cz)_{0.45}(DBT)_{0.55} (◇), and PTDBT (★).

with increasing DBT content could be due to the stronger donor- π -acceptor characteristic and more efficient intramolecular charge transfer. As shown in Fig. 2(b), the absorption bands of the PTs as thin films were located between 350 and 650 nm. More red shift of the maximum absorption wavelengths and absorption edges was observed for these polymers as solid films than those in *o*-DCB. Bandgap energies (E_g s) of the conjugated PTs were determined from the onset wavelengths of their absorption bands. As shown in Table 1, the values of E_g were in the following order: PT*t*Cz (1.97) > PT(*t*Cz)_{0.9}(DBT)_{0.1} (1.96) > PT(*t*Cz)_{0.64}(DBT)_{0.36} (1.90) = PT(*t*Cz)_{0.45}(DBT)_{0.55} (1.90) > PTDBT (1.87) (eV). The E_g decreased with an increasing molar ratio of DBT in the PTs. In solution, these polymers exhibited absorption edges ranging from 550 to 580 nm which underwent a 50–70 nm red shift in the solid state. Interestingly, the PTDBT film revealed a broad and strong absorption band in the region from 350 to 650 nm, covering the UV and visible regions. This is because the incorporation of the electron-deficient DBT group results in a smaller E_g of the polymer. With increasing the DBT contents of the PTs, the stronger donor- π -acceptor characteristic and more efficient intramolecular charge transfer between the polymer backbones to conjugated pendants were manifested. Herein, the absorbance edge was extended from 570 to 650 nm for the PTs when the DBT content was increased to a certain extent. This indicates that using geometric donor- π -acceptor conjugated moieties as pendants in PTs is a feasible strategy to adjust the E_g of conjugated polymers. In other words, the photophysical properties can be tailored for the pursuit of better photovoltaic performance *via* the variation of the molar ratios of conjugated pendants.

Table 1 Optical properties and electronic energy levels of the PT-based random copolymers comprising donor and acceptor pendants

| PTs | UV-visible absorption spectra | | | | Cyclic voltammetry | | | | |
|--|---|---|---|--------------------------------------|------------------------------------|------------------------|-------------------------------------|------------------------|-------------------------------------|
| | $\lambda_{\max}^{\text{abs}}$ (nm) ^a | $\lambda_{\max}^{\text{abs}}$ (nm) ^b | $\lambda_{\text{onset}}^{\text{abs}}$ (nm) ^b | E_g^{opt} (eV) ^c | $E_{\text{onset}}^{\text{ox}}$ (V) | HOMO (eV) ^d | $E_{\text{onset}}^{\text{red}}$ (V) | LUMO (eV) ^e | E_g^{ec} (eV) ^f |
| PTtCz | 415 | 421 | 629 | 1.97 | 0.95 | -5.39 | -1.31 | -3.13 | 2.26 |
| PT(<i>t</i> Cz) _{0.9} (DBT) _{0.1} | 433 | 475 | 634 | 1.96 | 0.87 | -5.31 | -1.30 | -3.14 | 2.17 |
| PT(<i>t</i> Cz) _{0.64} (DBT) _{0.36} | 440 | 502 | 654 | 1.90 | 0.85 | -5.29 | -1.26 | -3.18 | 2.11 |
| PT(<i>t</i> Cz) _{0.45} (DBT) _{0.55} | 450 | 517 | 655 | 1.90 | 0.84 | -5.28 | -1.23 | -3.21 | 2.07 |
| PTDBT | 461 | 550 | 687 | 1.80 | 0.82 | -5.26 | -1.12 | -3.32 | 1.94 |

^a The maximal absorption wavelength of the PTs in *o*-DCB. ^b The maximal absorption wavelength of the PTs as thin films. ^c Calculated from the onset absorption (λ_{onset}) of polymer thin films: $= 1240/\lambda_{\text{onset}}$. ^d The HOMO energy levels were obtained from the equation: $\text{HOMO} = -e(E_{\text{onset}}^{\text{ox}} - E_{\text{onset,ferrocene}}^{\text{ox}} + 4.8)$ (eV). ^e The LUMO levels of polymer were obtained from the equation: $\text{LUMO} = -e(E_{\text{onset}}^{\text{red}} - E_{\text{onset,ferrocene}}^{\text{red}} + 4.8)$ (eV). ^f Electrochemical bandgap energies $E = \text{LUMO} - \text{HOMO}$ (eV).

Electrochemical properties of the conjugated polymers

Since the PV performance of PSCs is closely related to the energy levels of the conjugated polymer, we determined the onset oxidation/reduction potentials of the PTs in air by employing cyclic voltammetry to calculate the HOMO/LUMO energy levels. This onset is defined by the intersection of the extrapolated baseline with the tangent to the inflection point. In Fig. 3, the onset oxidation potentials (E) of PTtCz, PT(*t*Cz)_{0.9}(DBT)_{0.1}, PT(*t*Cz)_{0.64}(DBT)_{0.36}, PT(*t*Cz)_{0.45}(DBT)_{0.55}, and PTDBT were 0.95, 0.87, 0.85, 0.84 and 0.82 V, respectively. The HOMO energy levels were calculated and listed in the order as following: PTtCz, (-5.39) < PT(*t*Cz)_{0.9}(DBT)_{0.1}, (-5.31) < PT(*t*Cz)_{0.64}(DBT)_{0.36}, (-5.29) < PT(*t*Cz)_{0.45}(DBT)_{0.55}, (-5.28) < PTDBT, (-5.26) (eV) (Table 1). These numbers are in an ideal range to ensure better air-stability and larger attainable V_{oc} in the device.³⁶ The onset reduction potentials (E) of PTtCz, PT(*t*Cz)_{0.9}(DBT)_{0.1}, PT(*t*Cz)_{0.64}(DBT)_{0.36}, PT(*t*Cz)_{0.45}(DBT)_{0.55}, and PTDBT were -1.31, -1.30, -1.26, -1.23, and -1.12 V, respectively. The LUMO energy levels were calculated and listed in the order as following: PTtCz, (-3.13) > PT(*t*Cz)_{0.9}(DBT)_{0.1}, (-3.14) > PT(*t*Cz)_{0.64}(DBT)_{0.36}, (-3.18) > PT(*t*Cz)_{0.45}(DBT)_{0.55},

(-3.21) > PTDBT, (-3.32) (eV). The electrochemical bandgap energies (E_g^{ec}) were calculated from the differences between the LUMO and HOMO energy levels (Table 1). The variations of electrochemical bandgap energies exhibited the same trend with those of the optical E_g s. The lower E_g^{ec} values for the PTs with an increasing content of DBT are attributed to the stronger donor- π -acceptor characteristic. The E_g^{ec} values of the studied PTs were 0.1–0.3 eV larger than the E_g^{opt} values, which is probably due to the presence of the exciton binding energy of conjugated polymers.³⁷ The HOMO levels of PTs were shifted to low-lying values by ca. 0.48–0.35 eV when compared to that of P3HT. It is known that attachment of the *tert*-butyl groups on the electrochemically active sites of aromatic amines leads to better electrochemical stability.³⁸ Additionally, the dihedral angles formed between the 9-position substituted carbazole and benzene plane were approximately 60 ° along with two bulky *tert*-butyl group substituents, which inhibit the close π - π aggregation effectively between the polymer main chains.^{39,40} On the other hand, two vicinal benzothiazolyl substituents of donor-acceptor-substituted fluorine fluorophores are nearly perpendicular to each other from X-ray structure analysis.²⁸ The rigid benzothiazolyl substituents prevent the fluorine molecules from π - π interaction. In this study, the most critical factor in tailoring the oxidation potentials was the incorporation of bulky conjugated pendants capable of twisting adjacent thiophene rings through steric interactions, thereby reducing the π orbital overlapping of PTs backbones and resulting in the deeper HOMO energy levels. This phenomenon was more pronounced in the *t*Cz-derived polymers. Deeper HOMO energy levels were observed while the *t*Cz content was increased. In contrast, a weak acceptor DBT group does not significantly affect the oxidation potentials.²⁸ However, the attachment of the electron withdrawing group (DBT) onto the polymer backbone also had a positive effect in obtaining lower HOMO energy levels, as compared to the parent P3HT.⁹ PTs with an increasing content of DBT were still able to retain satisfactory anti-oxidation stability as compared to the oxygen energy level (-5.2 eV with respect to vacuum).^{10,41} As mentioned previously, the LUMO energy level is strongly influenced by the acceptor moiety.²⁸ Apparently, the LUMO energy levels decreased with an increasing DBT content of PTs in a significant manner. Indeed,

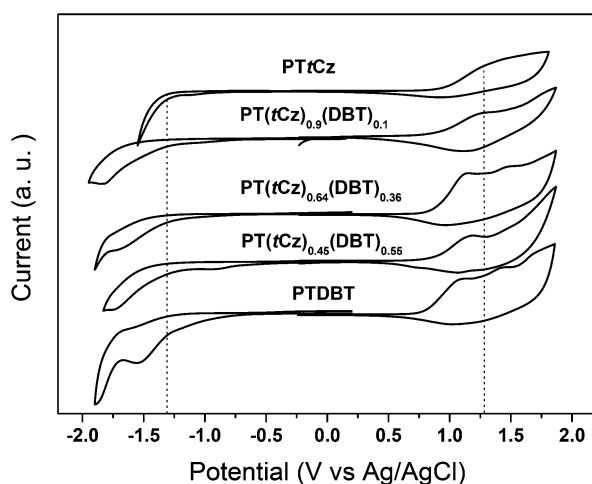


Fig. 3 Cyclic voltammograms of PT-based random copolymers thin films in a MeCN solution of 0.1 M TBAP at a scan rate of 50 mV S⁻¹.

the tunable energy levels of PTs were accomplished by incorporating both *t*Cz as donor pendants and DBT as acceptor pendants. This approach revealed a molecular design avenue to narrow the bandgap energies while retaining the low-lying HOMO levels.

PV properties of PSCs based on PT/PC₇₁BM films

PSCs were fabricated based on the ITO/PEDOT:PSS (30 nm)/PTs:PC₇₁BM/Ca (30 nm)/Al (100 nm) structure.³⁴ The optimum PTs/PC₇₁BM blend ratios were found to be 1 : 2.5 (w/w) and 1 : 3.5 (w/w) for PT*t*Cz-based and other PT-based photoactive films, respectively. Fig. 4 displays the *J*-*V* curves of each PTs/PC₇₁BM-based PSC, whereas the essential photovoltaic parameters (*V*_{oc}, *J*_{sc}, FF and PCE) are listed in Table 2. The devices based on PTs/PC₇₁BM all exhibited higher *V*_{oc} values (0.91–0.79 V), when compared with that of P3HT/PC₇₁BM (0.65 V).⁴² These high values of *V*_{oc} for the PT devices are consistent with their deeper HOMO energy levels. The *V*_{oc} value was decreased with increasing the DBT content in PTs, which is also consistent with the CV result. As expected, an excellent *V*_{oc} (0.91 V) value was observed for PT*t*Cz due to its deep HOMO energy level (−5.39 eV). Among these PT-based photoactive layers, the PT*t*Cz-based sample exhibited the best PCE (2.48%) because of its higher *J*_{sc} and largest *V*_{oc}, when compared with other samples in this study. One would have expected to further increase the PCE by introducing a DBT unit into the system. However, the PCE of PTDBT device was significantly limited by its low *J*_{sc} and *V*_{oc}, despite the fact that the UV-vis absorption spectrum of PTDBT was more red-shifted than that of PT*t*Cz. The results obtained in the PCE performances prompted us to further investigate the relevance of the charge transport properties of the PTs, which will be addressed in a later section. The lower photocurrent density might result from charge transport-related recombination losses. Additionally, the PCE of PT(*t*Cz)_{0.9}(DBT)_{0.1}/PC₇₁BM (0.89%) was the lowest among these PT-based PSCs. The presence of low molecular-weight fractions in the system (a rather broader PDI value (3.49) for PT(*t*Cz)_{0.9}(DBT)_{0.1}) would normally lead to a reduced

Table 2 Photovoltaic performances of the PTs/PC₇₁BM-based conventional PSCs

| PTs | <i>V</i> _{oc} (V) | <i>J</i> _{sc} (mA cm ^{−2}) | FF | PCE (%) |
|--|----------------------------|---|------|---------|
| PT <i>t</i> Cz ^a | 0.91 | 6.58 | 0.41 | 2.48 |
| PT(<i>t</i> Cz) _{0.9} (DBT) _{0.1} | 0.82 | 3.54 | 0.31 | 0.89 |
| PT(<i>t</i> Cz) _{0.64} (DBT) _{0.36} | 0.85 | 5.52 | 0.35 | 1.65 |
| PT(<i>t</i> Cz) _{0.45} (DBT) _{0.55} | 0.80 | 4.93 | 0.35 | 1.39 |
| PDBT | 0.79 | 5.05 | 0.33 | 1.31 |

^a PTs/PC₇₁BM = 1 : 2.5.

performance in photovoltaic parameters. It has been demonstrated that the broad molecular weight distributions of PTs are responsible for this dramatic decrease in performance, particularly those with low molecular weight fractions.⁴³ This phenomenon is caused by distinctly reduced charge carrier (hole) mobility in the donor phase of the devices built from the lower molecular-weight fractions of the PT samples.⁴⁴

Morphology of the thin films of PT/PC₇₁BM blends

The performance of a PSC is strongly dependent on the morphology of the conjugated polymer/fullerene derivative composite film. To generate more effective free carriers from bonding excitations and to avoid the recombination of excitons and free carriers, the P/N heterojunction phase must be controlled at the nanoscale level with an interpenetrating network. This is because the diffusion range of the exciton is approximately 10–20 nm.^{45,46} AFM was utilized to investigate the compatibility and morphology of the PT/PC₇₁BM composite films prepared in the same manner as those prepared in the device fabrication (Fig. 5, topographic (a) and phase (b) images). In each case, we observed a phase-separated interpenetrating network with sizable PC₇₁BM domains. The surface roughnesses of the PT/PC₇₁BM films were in the range of 0.21–0.32 nm. The overall small root mean square (RMS) values are probably due to the random conformation of the PTs and the presence of the steric bulky pendants in these PTs. These two factors prohibit the ordered packing of the polymer chains in the solid state.⁴⁷ The bulky pendants in the PTs provide sufficient free volume for the PC₇₁BM units to intercalate into the polymer chains. This could permit better compatibility between PC₇₁BM and the polymer chains. In Fig. 5(b), a certain degree of phase separation was observed, which is favorable for efficient formation of free carriers to provide optimal PV properties of PSCs. These results indicate that the compatibility and surface morphology of the PTs/PC₇₁BM films were influenced by the geometric structure of the pendants, but not by the presence of the electron donor or acceptor moieties.

Space charge limited current hole mobility

In addition to the morphology, we suspect that the variation of hole mobility might play an important role in influencing the device performance. To evaluate the contribution of polymer mobility, we employed hole-only devices using a high-work-function material, palladium (Pd), as the cathode to block the

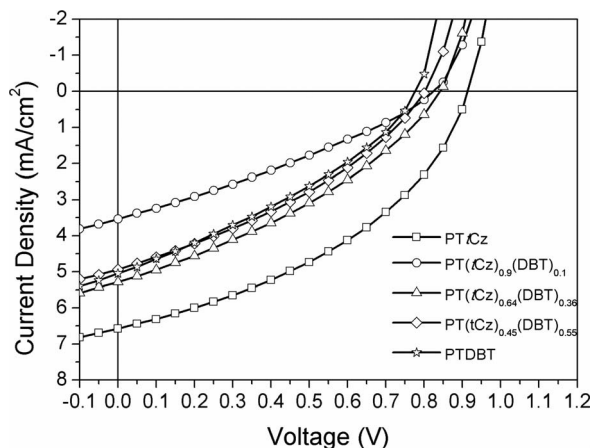


Fig. 4 Current density–potential curves of illuminated (AM 1.5 G, 100 mW cm^{−2}) PTs/PC₇₁BM-based conventional PSCs.

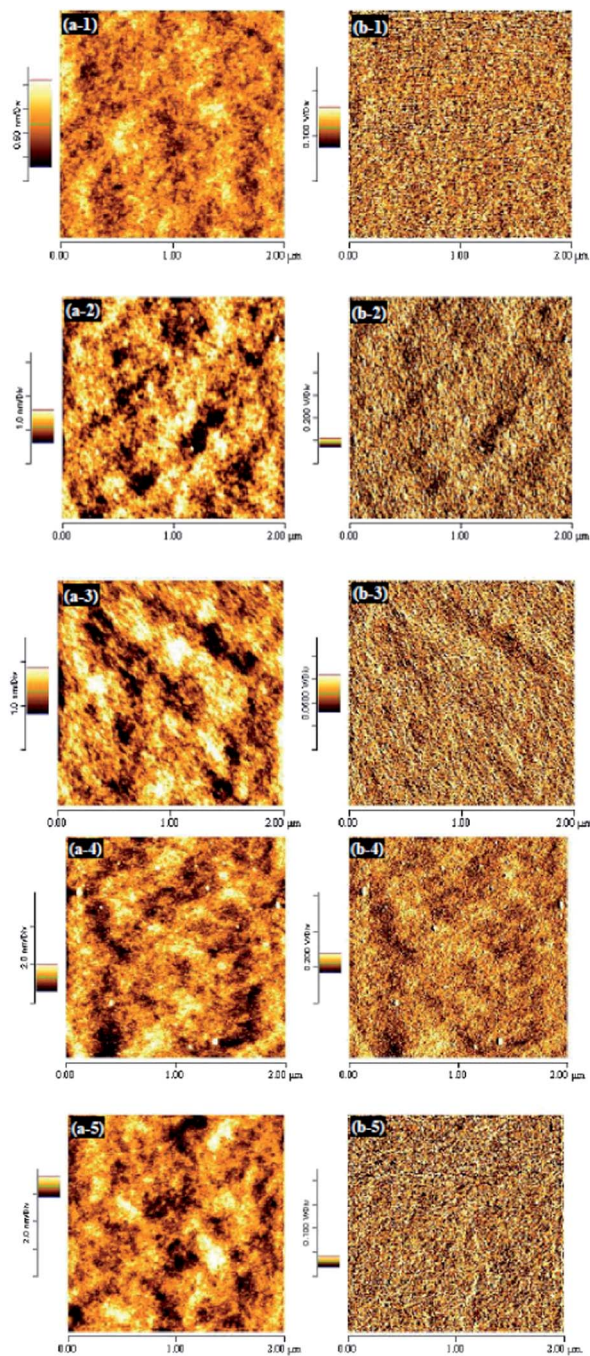


Fig. 5 AFM tapping mode topographic (a) and phase (b) images of fabricated photoactive PTs/PC₇₁BM-based blend thin films (1-PTtCz, 2-PT(tCz)_{0.9}(DBT)_{0.1}, 3-PT(tCz)_{0.64}(DBT)_{0.36}, 4-PT(tCz)_{0.45}(DBT)_{0.55}, and 5-PTDBT).

back injection of electrons.⁴⁸ When a sufficient voltage is applied to this hole-only device, the transport of holes through the polymer film is limited by the space charge that accumulates. The space charge limited current (SCLC) is described by eqn (1):

$$J = \frac{9}{8} \epsilon_r \epsilon_0 \mu_h \frac{V^2}{L^3} \quad (1)$$

Where ϵ_r is the dielectric constant of the polymer, ϵ_0 is the permittivity of free space, μ_h is the hole mobility, V is the voltage

applied to the device, and L is the blend film thickness. The experimental dark-current densities of the PTs devices were measured in the hole-only devices. The applied voltage was corrected for the built-in voltage (V_{BI}), which was estimated from the difference between the work function and the HOMO energy level of PTs. Based on the slopes from the plots of $J^{0.5}$ with respect to V for the corresponding devices, we calculated the field-independent mobilities of the PTtCz, PT(tCz)_{0.9}(DBT)_{0.1}, PT(tCz)_{0.64}(DBT)_{0.36}, and PT(tCz)_{0.45}(DBT)_{0.55} derived devices to be 1.35×10^{-5} , 9.19×10^{-6} , 9.23×10^{-6} , and 4.11×10^{-6} ($\text{cm}^2 \text{V}^{-1} \text{s}^{-1}$), respectively. With increasing the tCz content in the PTs, higher hole mobility values were observed, which is consistent with the PCE performance mentioned earlier. This is attributed to the electron-donating character and more efficient π - π^* charge transfer of the carbazole moiety, which has been widely used as a hole transport material for organic electronics.²⁶ The increase in hole mobility exerts more influence on the J_{sc} value of the PTs-derived PSCs than the absorption characteristics. On the contrary, the losing hole mobility and lowering J_{sc} values were consistent for the PTs with increasing DBT content. The SCLC measurements are in good agreement with the PCE performances. With increasing the DBT content in the PTs, the presence of lower hole mobilities would lead to unbalanced charge transport and hole accumulation. The hole accumulation partially acted as the recombination centers of electron-hole pairs. Subsequently the photocurrent collection efficiency of the respective electrode was restricted.

Air stability of the PTtCz-derived inverted device

Our interests in understanding the air stability of our rationally designed low HOMO materials led us to evaluate their PCE degradation with time under ambient conditions. Due to the better environmental stability of the inverted cells,^{49–52} we further studied the durability of the PTtCz/PC₇₁BM-based film based on an inverted structure of ITO/ZnO_x/PTtCz:PC₇₁BM/MoO₃/Ag, as shown in Fig. 6(a). The long-term current density-potential characteristics of the PTtCz-derived inverted devices without encapsulation under ambient condition is shown in Table 3. The evaluated photovoltaic characteristics of the PTtCz/PC₇₁BM-based devices, as a function of elapsed time, are shown in Fig. 6(b). For each set of points in the plot, the average performance parameters of the devices were measured, and the standard deviation was recorded over an extended period of testing, further testifying the uniformity and robustness of the devices. As expected, the low-lying HOMO level of PTtCz (−5.39 eV), which is relatively stable against oxidation in ambient conditions allowed the device to retain *ca.* 80% of its original efficiency over a period of 1032 h (ISOS-D-1 shelf).^{30,31} Preliminary results indicate that this new synthetic material exhibited good stability in ambient conditions (defined as 25 °C/RH 50% in general) using an air-stable inverted architecture. Nevertheless, factors such as heat and humidity would affect the OPV performance in long-term practical applications.⁵³ Therefore, further long-term stability investigations are currently underway to understand the performance of inverted devices under outdoor conditions (ISOS-O-1 shelf).³¹

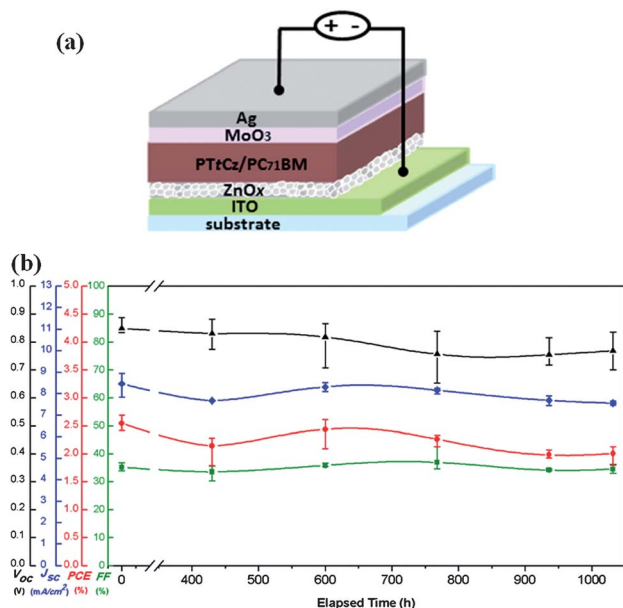


Fig. 6 (a) Architecture of the PTtCz/PC₇₁BM-based inverted PSC. (b) Summary plots for the long-term photovoltaic performances in ambient condition without encapsulation of the PTtCz/PC₇₁BM-based inverted PSC.

Table 3 Long-term photovoltaic performances of the PTtCz/PC₇₁BM-based inverted PSC in ambient conditions without encapsulation

| Time (h) | V_{oc} (V) | J_{sc} (mA cm ⁻²) | FF | PCE (%) | Efficiency decay (%) ^a |
|----------|--------------|---------------------------------|------|---------|-----------------------------------|
| 0 | 0.86 | 8.43 | 0.36 | 2.58 | — |
| 430 | 0.85 | 7.67 | 0.35 | 2.26 | 12 |
| 600 | 0.85 | 8.30 | 0.36 | 2.55 | 1 |
| 768 | 0.76 | 8.13 | 0.38 | 2.30 | 11 |
| 936 | 0.76 | 7.68 | 0.34 | 1.98 | 23 |
| 1032 | 0.77 | 7.56 | 0.35 | 2.01 | 22 |

^a Based on its original conversion efficiency (0 h).

Conclusion

In conclusion, we synthesized a series of PT-based random copolymers functionalized with different composition ratios of tCz and DBT as bipolar pendant groups *via* Stille copolymerization. The dual-adjusted strategy towards narrow (1.97 to 1.80 eV) and lower-lying HOMO levels (−5.39 to −5.26 eV) of PTs were accomplished by incorporating both electron donor-tCz and acceptor-DBT pendants onto PTs. As expected, each PTs/PC₇₁BM PSC exhibited significantly high V_{oc} values (0.91 to 0.79 V) in the conventional device fabrication. The PSC based on PTtCz/PC₇₁BM (w/w = 1 : 2.5) reached a PCE of 2.48% under the illumination of AM 1.5, 100 mW cm⁻², along with a V_{oc} of 0.91 V, a J_{sc} of 6.58 mA cm⁻², and a FF of 41%. An inverted PSC without encapsulation based on PTtCz/PC₇₁BM as a photoactive layer, was capable of retaining *ca.* 80% of its original efficiency for 1032 h, according to the ISOS-D-1 shelf protocol. The excellent V_{oc} value for a long-term air stable inverted PSC based on a PT-type polymer using PCBM as an acceptor was achieved in this study.

Acknowledgements

We thank the National Science Council of Taiwan for financial support (grant numbers NSC-101-2221-E-002-035-MY3 and NSC101-2113-M-131-001-MY2).

Notes and references

- 1 D. Angmo, T. T. Larsen-Olsen, M. Jørgensen, R. R. Søndergaard and F. C. Krebs, *Adv. Energy Mater.*, 2013, **3**, 172.
- 2 N. Espinosa, M. Hosel, D. Angmo and F. C. Krebs, *Energy Environ. Sci.*, 2012, **5**, 5117.
- 3 X. Li, W. C. H. Choy, L. Huo, F. Xie, W. E. I. Sha, B. Ding, X. Guo, Y. Li, J. Hou, J. You and Y. Yang, *Adv. Mater.*, 2012, **24**, 3046.
- 4 L. Dou, J. You, J. Yang, C. C. Chen, Y. He, S. Murase, T. Moriarty, K. Emery, G. Li and Y. Yang, *Nat. Photonics*, 2012, **6**, 180.
- 5 Z. C. He, C. M. Zhong, S. J. Su, M. Xu, H. Wu and Y. Cao, *Nat. Photonics*, 2012, **6**, 591.
- 6 W. Ma, C. Yang, X. Gong, K. Lee and A. J. Heeger, *Adv. Funct. Mater.*, 2005, **15**, 1617.
- 7 Y. Kim, S. Cook, S. M. Tuladhar, S. A. Choulis, J. Nelson, J. R. Durrant, D. C. C. Bradley, M. Giles, I. McCulloch, C. S. Ha and M. Ree, *Nat. Mater.*, 2006, **5**, 197.
- 8 Y. J. Cheng, S. H. Yang and C. S. Hsu, *Chem. Rev.*, 2009, **109**, 5868.
- 9 G. Dennler, M. Scharber and C. J. Brabec, *Adv. Mater.*, 2009, **21**, 1323.
- 10 D. M. Leeuw, M. M. J. Simenon, A. R. Brown and R. E. F. Einerhand, *Synth. Met.*, 1997, **87**, 53.
- 11 Y. Li and Y. Zou, *Adv. Mater.*, 2008, **20**, 2952.
- 12 Y. Li, *Acc. Chem. Res.*, 2012, **45**, 723.
- 13 J. Hou, Z. A. Tan, Y. Yan, Y. He, C. Yang and Y. Li, *J. Am. Chem. Soc.*, 2006, **128**, 4911.
- 14 Z. G. Zhang, S. Zhang, J. Min, C. Chui, J. Zhang, M. Zhang and Y. Li, *Macromolecules*, 2011, **45**, 113.
- 15 J. H. Tsai, W. Y. Lee, W. C. Chen, C. Y. Yu, G. W. Hwang and C. Ting, *Chem. Mater.*, 2010, **22**, 3290.
- 16 C. Y. Yu, B. T. Ko, C. Ting and C. P. Chen, *Sol. Energy Mater. Sol. Cells*, 2009, **93**, 613.
- 17 Y. T. Chang, S. L. Hsu, M. H. Su and K. H. Wei, *Adv. Mater.*, 2009, **21**, 2093.
- 18 Y. T. Chang, S. L. Hsu, G. Y. Chen, M. H. Su, T. A. Singh, W. G. Diao and K. H. Wei, *Adv. Funct. Mater.*, 2008, **18**, 2356.
- 19 Z. G. Zhang, S. Y. Zhang, J. Min, C. H. Chui, J. Zhang, M. J. Zhang and Y. Li, *Macromolecules*, 2012, **45**, 113.
- 20 H. J. Wang, L. H. Chan, C. P. Chen, S. L. Lin, R. H. Lee and R. J. Jeng, *Polymer*, 2011, **52**, 326.
- 21 H. J. Wang, L. H. Chan, C. P. Chen, R. H. Lee, W. C. Su and R. J. Jeng, *Thin Solid Films*, 2011, **519**, 5264.
- 22 H. J. Wang, J. Y. Tzeng, C. W. Chou, C. Y. Huang, R. H. Lee and R. J. Jeng, *Polym. Chem.*, 2013, **3**, 506.
- 23 H. J. Wang, Y. P. Chen, Y. C. Chen, C. P. Chen, R. H. Lee, L. H. Chan and R. J. Jeng, *Polymer*, 2012, **53**, 4091.

- 24 S. Ko, E. T. Hoke, L. Pandey, S. Hong, R. Mondal, C. Risko, Y. Yi, R. Noriega, M. D. McGehee, J. L. Brédas, A. Salleo and Z. Bao, *J. Am. Chem. Soc.*, 2012, **134**, 5222.
- 25 O. Kwon, S. Barlow, S. A. Odom, L. Beverina, N. J. Thompson, E. Zojer, J. L. Brédas and S. R. Marder, *J. Phys. Chem. A*, 2005, **109**, 9346.
- 26 S. L. Lin, L. H. Chan, R. H. Lee, M. Y. Yen, W. J. Kuo, C. T. Chen and R. J. Jeng, *Adv. Mater.*, 2008, **20**, 3947.
- 27 C. L. Chiang, C. F. Shu and C. T. Chen, *Org. Lett.*, 2005, **7**, 3717.
- 28 C. L. Chiang, Y. J. Wen, Y. S. Wen, C. F. Shu and C. T. Chen, *J. Chin. Chem. Soc.*, 2006, **53**, 1325.
- 29 X. Zhang, T. T. Steckler, R. R. Dasari, S. Ohira, W. J. Potscavage Jr, S. P. Tiwari, S. Coppée, S. Ellinger, S. Barlow, J. L. Brédas, B. Kippelen, J. R. Reynolds and S. R. Marder, *J. Mater. Chem.*, 2010, **20**, 123.
- 30 M. O. Reese, S. A. Gevorgyan, M. Jørgensen, E. Bundgaard, S. R. Kurtz, D. S. Ginley, D. C. Olson, M. T. Lloyd, P. Morvillo, E. A. Katz, A. Elschner, O. Haillant, T. R. Currier, V. Shrotriya, M. Hermenau, M. Riede, K. R. Kirov, G. Trimmel, T. Rath, O. Inganäs, F. Zhang, M. Andersson, K. Tvingstedt, M. Lira-Cantu, D. Laird, C. McGuinness, S. Gowrisanker, M. Pannone, M. Xiao, J. Hauch, R. Steim, D. M. DeLongchamp, R. Rösch, H. Hoppe, N. Espinosa, A. Urbina, G. Yaman-Uzunoglu, J. Bonekamp, A. J. J. M. van Breemen, C. Girotto, E. Voroshazi and F. C. Krebs, *Sol. Energy Mater. Sol. Cells*, 2011, **95**, 1253.
- 31 M. Jørgensen, K. Norrman, S. A. Gevorgyan, T. Tromholt, B. Andreasen and F. C. Krebs, *Adv. Mater.*, 2012, **24**, 580.
- 32 A. C. Spivey, D. J. Turner, M. L. Turner and S. Yeates, *Org. Lett.*, 2002, **4**, 1899.
- 33 Y. J. Cheng, J. S. Wu, P. I. Shih, C. Y. Chang, P. C. Jwo, W. S. Kao and C. S. Hsu, *Chem. Mater.*, 2011, **23**, 2361.
- 34 C. P. Chen, Y. D. Chen and S. C. Chuang, *Adv. Mater.*, 2011, **23**, 3859.
- 35 Y. W. Li, H. J. Xia, B. Xu, S. P. Wen and W. J. Tian, *J. Polym. Sci., Part A: Polym. Chem.*, 2008, **46**, 3970.
- 36 M. C. Scharber, D. Mühlbacher, M. Koppe, P. Denk, C. Waldauf, A. J. Heeger and C. J. Brabec, *Adv. Mater.*, 2006, **18**, 789.
- 37 Y. Zhu, F. S. Kim, R. D. Champion and S. A. Jenekhe, *Macromolecules*, 2008, **411**, 7021.
- 38 H. M. Wang, S. H. Hsiao, G. S. Liou and C. H. Sun, *J. Polym. Sci., Part A: Polym. Chem.*, 2010, **48**, 4775.
- 39 Z. Ning, Q. Zhang, W. Wu, H. Pei, B. Liu and H. Tian, *J. Org. Chem.*, 2008, **73**, 3791.
- 40 D. J. Liaw, B. Y. Liaw, L. J. Li, B. Sillion, R. Mercier, R. Thiria and H. Sekiguchi, *Chem. Mater.*, 1998, **10**, 734.
- 41 R. Y. Mahale, A. Arulkashmir, K. Dutta and K. Krishnamoorthy, *Phys. Chem. Chem. Phys.*, 2012, **14**, 4577.
- 42 C. P. Chen, S. H. Chan, T. C. Chao, C. Ting and B. T. Ko, *J. Am. Chem. Soc.*, 2008, **130**, 12828.
- 43 R. C. Hiorns, R. de Bettignies, J. Leroy, S. Bailly, M. Firon, C. Sentein, H. Preud'homme and C. DagronLartigau, *Eur. Phys. J.-Appl. Phys.*, 2006, **36**, 295.
- 44 P. Schilinsky, U. Asawapirom, U. Scherf, M. Biele and C. J. Brabec, *Chem. Mater.*, 2005, **17**, 2175.
- 45 A. C. Mayer, S. R. Scully, B. E. Hardin, M. W. Rowell and M. D. McGehee, *Mater. Today*, 2007, **10**, 28.
- 46 S. R. Scully and M. D. McGehee, *J. Appl. Phys.*, 2006, **100**, 034907.
- 47 W. W. Li, Y. Han, Y. L. Chen, C. H. Li, B. S. Li and Z. S. Bo, *Macromol. Chem. Phys.*, 2010, **211**, 948.
- 48 C. P. Chen, Y. C. Chen and C. Y. Yu, *Polym. Chem.*, 2013, **4**, 1161.
- 49 C. Y. Li, T. C. Wen, T. H. Lee, T. F. Guo, J. C. A. Huang, Y. C. Lin and Y. J. Hsu, *J. Mater. Chem.*, 2009, **19**, 1643.
- 50 S. Chen, C. E. Small, C. M. Amb, J. Subbiah, T. H. Lai, S. W. Tsang, J. R. Manders, J. R. Reynolds and F. So, *Adv. Energy Mater.*, 2012, **2**, 1333.
- 51 Z. Tan, D. Qian, W. Zhang, L. Li, Y. Ding, Q. Xu, F. Wang and Y. Li, *J. Mater. Chem. A*, 2013, **1**, 657.
- 52 H. L. Yip and A. K. Y. Jen, *Energy Environ. Sci.*, 2012, **5**, 5994.
- 53 M. Manceau, E. Bundgaard, J. E. Carlé, O. Hagemann, M. Helgesen, R. Søndergaard, M. Jørgensen and F. C. Krebs, *J. Mater. Chem.*, 2011, **21**, 4132.